Composites: Part A 181 (2024) 108151

Contents lists available at ScienceDirect

Composites Part A

journal homepage: www.elsevier.com/locate/compositesa

Properties of shape memory polyimide composites with continuous "brick-and-mortar" layered structure: High flame retardancy, ablation resistance, and high mechanical properties

Xiaofei Wang [a], Yang He [a], Xinli Xiao [b], Yanju Liu [c], Jinsong Leng [a,*]

[a] National Key Laboratory of Science and Technology on Advanced Composites in Special Environments, Harbin Institute of Technology, Harbin 150080, PR China
[b] MIIT Key Laboratory of Critical Materials Technology for New Energy Conversion and Storage, School of Chemistry and Chemical Engineering, Harbin Institute of Technology, Harbin, 150001, PR China
[c] Department of Astronautic Science and Mechanics, Harbin Institute of Technology, Harbin 150001, PR China

ARTICLE INFO

Keywords:
A. Polymer-matrix composites (PMCs)
A. Smart materials
B. High-temperature properties
B. Microstructures

ABSTRACT

Shape memory polymer (SMP) is a type of smart materials mostly working below 200 ℃, which is difficult to be applied in the ultra-high temperature, even 1000 ℃. Herein, we have prepared shape memory polyimide composites (SMPIC) inspired by nacre "brick-and-mortar" layered structure. The SMPIC has the flame-retardant grade of V0 and the limiting oxygen index of 53.1% when the flame retardants amount is 20%. Besides, it has excellent resistance to high temperature airflow erosion, and the mass ablation ratio is 0.0053 g/s. After rapid thermal processing at 1000 ℃, the mechanical strength is 100 MPa, and the strength retention ratio is 103.3%. Also, the simple actuator can overturn iron blocks that are more than 8 times of its own weight, thus, the smart composite has huge application prospects in the high temperature environment, such as active morphing re-entry parachute, which provides reference for lightweight smart structures.

1. Introduction

Shape memory polymer (SMP) is an intelligent material that can maintain a temporary shape after shaping and return to the original shape under external stimuli, such as heat, light, electricity, magnetism or chemistry solvent, etc. [1–6]. In 2023, Xie et al. reported a four-dimensional printable shape memory hydrogel with shape-shifting onset adjustable by changing the programming conditions, and it could undergo shape transformation at natural ambient temperature [7]. Thomas et al. designed a magnetically actuated variable stiffness manipulator (VSM) based on deployable shape memory polymer springs. The VSM could be deployed in a compact form and extended to achieve variable bending curvatures in soft and rigid states, which could facilitate instrument insertion and reduce operation invasiveness, and had potential clinical applications [8]. By designing molecular chain segments, many polymers exhibit shape memory effects, such as shape memory polyimide, shape memory epoxy resin, and shape memory polyurethane, etc. Shape memory polyimide (SMPI) and composites are expected to be used in smart actuators, active deformable structures and aerocraft skin, etc. because of its outstanding shape memory properties, radiation resistance, thermal stability and mechanical performances [9–14]. Polyimide (PI) is a self-extinguishing polymer, which can meet flame-retardant requirements in most fields. When exposed to the fire, it can be carbonized and had no toxic, no molten droplets and self-extinguishing out of fire [15–17]. Xu et al. prepared polyimide composites with high flame retardancy and mechanical properties, when the red phosphorus hybrid graphene amount was 2.2 wt%, the limit oxygen index (LOI) was as high as 39.4% [18]. However, the flame retardancy requirements are harsher in some special fields, for example, traditional PI is difficult to resist high-temperature airflow erosion in 1000 ℃ environment, leading to the thermal protection failure [19,20]. At present, there is no report on the flame retardancy of SMPI, thus, developing SMPI with extreme high temperature resistance is of great significance.

Nacre is a kind of bioceramics, which was composed by highly ordered aragonite ($CaCO_3$) layers and small amount of biological proteins, exhibiting "brick-and-mortar" micro-nano structures and great mechanical properties. Inspired by the natural nacre structures, USTC's Yu et al. constructed nacreous bulk nanocomposites with tunable mechanical properties by introducing multiscale soft-rigid polymer dual-

* Corresponding author.
E-mail address: lengjs@hit.edu.cn (J. Leng).

https://doi.org/10.1016/j.compositesa.2024.108151
Received 24 July 2023; Received in revised form 22 February 2024; Accepted 15 March 2024
Available online 17 March 2024

networks [21]. Besides, Yu et al. reported a kind of nacre-inspired bacterial cellulose (BC)/synthetic mica nanopaper with excellent mechanical properties and highly resistant to alternating high and low temperatures, UV light, and atomic oxygen, making it an ideal candidate for extreme environment-resistant materials [22]. Herein, we prepared the world's first flame-retardant SMPI composite with continuous "brick-and-mortar" layered structure which was inspired by the microstructure of nacre, specifically, the SMPI/flame retardant composite was equivalent to the "soft mortar" layer and the SMPI/carbon fiber composite was equivalent to the "hard brick" layer. We characterized the mechanical strength after rapid thermal processing, flame retardancy and ablation resistance, to verify its feasibility in 1000 ℃ environment.

Hydroxide flame retardant possesses a characteristic of environmental friendliness, because it does not produce any harmful substances and the decomposition products can absorb harmful gases generated by the composites during the combustion process [23,24]. $Mg(OH)_2$ is a type of filled flame retardant, when the temperature exceeds 350 ℃, it could lose water and transform into MgO, meanwhile, it absorbs CO_2 in the air and forms $5MgO \cdot 4CO_2 \cdot xH_2O$. MgO has a melting point of 2852 ℃ and a boiling point of 3600 ℃, which possesses a highly fire-resistant performance, and it can be transformed into crystals over 1000 ℃ burning environment and become a kind of sintered MgO on 1500 ℃ [25–27]. Therefore, the decomposed MgO is a good refractory material, which improves the fire resistance of the composite, at the same time, the water vapor is also used as a smoke suppressant. Carbon fiber (CF) is a kind of high strength and high modulus fiber, of which the theoretical temperature resistance exceeds 2600 ℃, so, it is a promising material to manufacture high-tech facilities like aircraft engine components [28,29]. In addition, SiO_2 possesses excellent fire resistance performance with a melting point of 1723 ℃ and a boiling point of 2230 ℃, which covers on the matrix material surface together with the flame retardant to prevent the flame from extending to the material interior [30].

In this paper, aromatic heterocyclic diamines containing imidazoles and biphenyl dianhydride are polycondensated together, which is then compounded with carbon fiber fabric to obtain a polyamide acid/carbon fiber fabric composite (PAA/CF). Innovatively, the PAA/flame retardant and PAA/CF are overlapped layer by layer, and then through hot pressing and secondary thermal amination, the flame-retardant shape memory polyimide composites (SMPIC) with continuous "brick-and-mortar" layered microstructures are produced. The SMPI/flame retardant is equivalent to the "soft mortar" layer and the SMPI/CF is equivalent to the "hard brick" layer, which is similar to the nacre microstructure and achieves good flame retardancy, ablation resistance and high mechanical properties. The SMPIC has rapid-actuating shape memory performance, which lays a foundation for the application of intelligent materials in high temperature environment, even 1000 ℃, such as, active deformation wings, autonomous deformation skin structures, and re-entry parachute, etc.

2. Experiment

2.1. Materials

3,3',4,4'-Biphenyltetracarboxylic dianhydride (BPDA), 5-amino-2-(4-aminophenyl) benzimidazole (DAPBI), $Mg(OH)_2$ flame retardant (> 99.0%), and SiO_2 nanoparticle (30 nm in diameter) were all bought from Shanghai Aladdin Co., Ltd. Ethanol and dimethyl sulfoxide (DMSO) were both from Tianjin Fengchuan Chemical Reagent Technology Co., Ltd. Carbon-fiber twill fabric (T300-3K) was purchased from Japan Toray Co., Ltd.

2.2. Preparation of flame-retardant shape memory polyimide composite

(I) DAPBI was dissolved in the DMSO solvent at 25 ℃ environment, then, BPDA was also dissolved in the solution (The molar ratio of DAPBI to BPDA was 1:1.), and the mechanical mixing speed was 200-500 r/min for 120 h, N_2 atmosphere, to fabricate a polyamic acid solution (PAA) which was divided into two equal parts.

(II) $Mg(OH)_2$ and SiO_2 were added into one part of the PAA solution, and stirred for 3 h to mix them evenly. The mass fraction of $Mg(OH)_2$ was 10 wt%, 15 wt%, 20 wt%, 25 wt%, and 30 wt% of whole PAA, respectively, and the mass fraction of SiO_2 was 5 wt% of whole PAA.

(III) The carbon fiber was soaked into the other part of PAA solution in 50 °C environment for 12 h, until the DMSO was evaporated entirely, and PAA/CF composite was produced.

(IV) The PAA/flame retardant solution obtained by step (II) was poured onto the surface of the PAA/CF composite obtained by step (III), and it was placed in a vacuum oven to remove the solvent.

(V) The PAA/flame retardant composite and PAA/CF composite obtained by step (IV) were stacked layer by layer and was pre-pressed by a hot press to form composite materials with continuous "brick-and-mortar" structures. The pre-pressing conditions was 180 ℃ for 10 min and 250 ℃ for 60 min, and the pressure was 3-5 MPa, and the thickness was 0.5-1.5 mm.

(VI) The pre-pressed composites obtained by step (V) were cured secondary, and the flame-retardant SMPICs were fabricated by heating to 250 °C for 2 h and 300 °C for 3 h, named as SMPIC-10, SMPIC-15, SMPIC-20, SMPIC-25, and SMPIC-30, respectively. The chemical reaction route and manufacturing process were exhibited in Fig. 1.

2.3. Characterizations

Dynamic mechanical performance of SMPIC was tested by DMA Q800 (TA Corporation, USA). Test conditions included stretch test mode, 1 Hz frequency, 0.2 % amplitude, N_2 flow rate of 10.00 mL / min, and the temperature range of 25-560 ℃. Thermal stability of SMPIC was characterized by TGA / DSC1 thermal analyzer (METTLER-TOLEDO Corporation, Switzerland), and the residual amount at 800 ℃ was utilized to determine the thermal stability of the composites. Test conditions were that the weight was 5-10 mg, N_2 flow rate was 10.00 mL / min, the temperature range was 25-800 ℃, and the heating rate was 10 ℃ / min. The flame retardancy of SMPIC was characterized by ZY6155 oxygen index measuring instrument (Taiwan Songshu Corporation, China). In the testing process, O_2 concentration was increased from 40% until the sample burned, and the critical value of O_2 concentration closest to the burning was taken as the limiting oxygen index (LOI). The vertical combustibility and flame retardant grade were evaluated by GB2409-84 standard and UL94-2009 standard, respectively. The molecular chemical groups in the ablation central region, transition region and heat affect region of the ablated SMPIC composite were characterized by FTIR spectrometer, and the wavelength range was 4000-500 cm^{-1}. According to the GJB323A-96 standard, the mass ablation ratio of SMPIC at 1350 ℃ was tested by a cassette furnace ablation equipment. The ablation time was 5 s, 10 s, 15 s, 20 s, 25 s, and 30 s. The analytical balance weighed the original mass m_1 and the mass m_2 after ablation, and the mass ablation rate R_m was calculated as follows:

$$R_m = \frac{m_2 - m_1}{\Delta t} \cdots\cdots \quad (1)$$

SEM-EDS (JEM-1200, JEOL Company, Japan) was utilized to characterize the surface morphology and elements of the ablation central region, transition region and heat affect region of the SMPIC after ablation. The 3D laser confocal microscope (OLS4100, Japan) was also used to characterize the surface morphology of the SMPIC after ablation. Based on the GB/T 30873-2014 standard, the mechanical strength of SMPIC was tested after the rapid thermal processing. Specifically, the sample was heated in a silicon molybdenum rod muffle furnace for 30 s, and the temperature differences were 600 ℃, 800 ℃, 1000 ℃ and 1350 ℃, respectively. Then, the sample was taken out and was put into the 0 ℃ environment for rapid cooling. The residual strength was tested by Zwick tensile testing machine, and the tensile rate was 5 mm / min. The

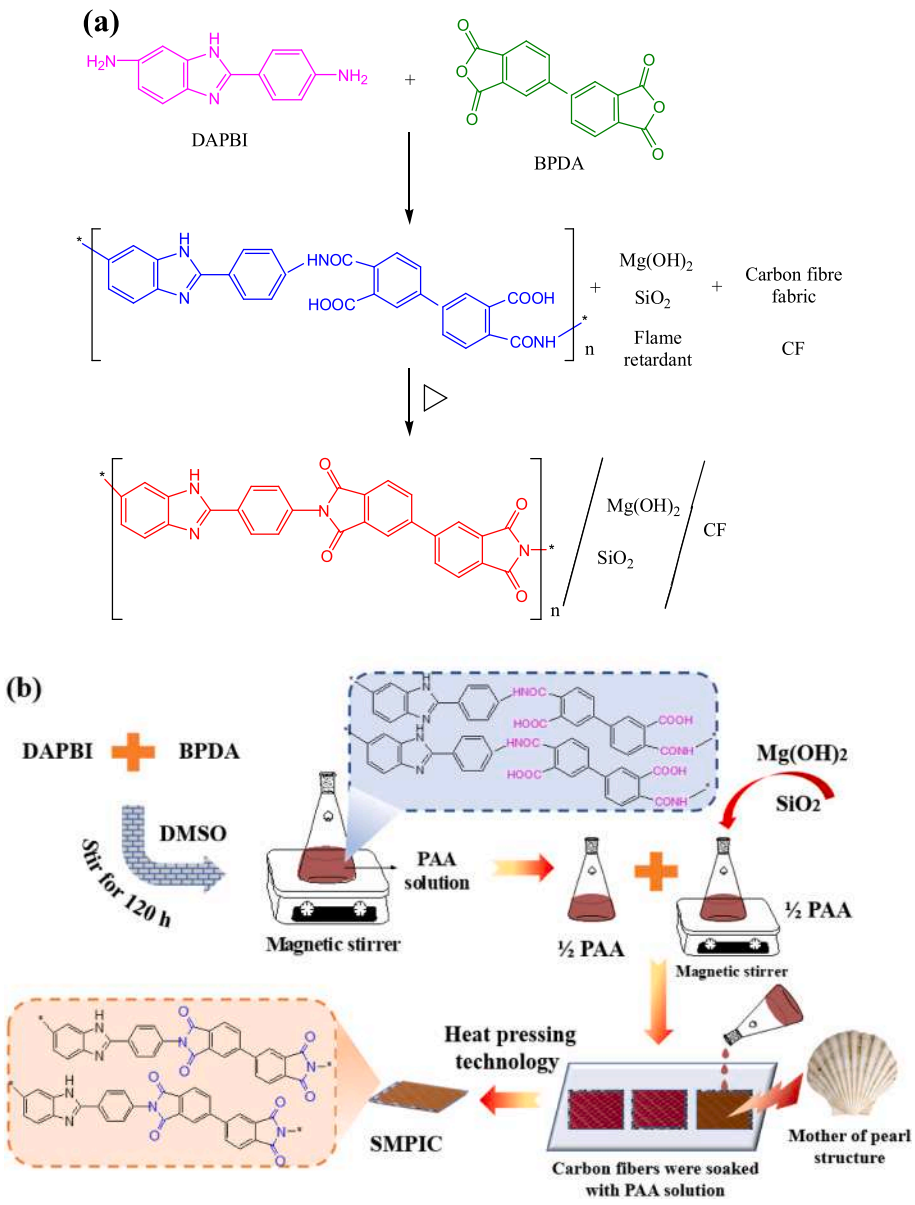

Fig. 1. (a) The synthesis route of SMPIC, (b) schematic diagram of SMPIC preparation process.

"brick-and-mortar" layered structure of the SMPIC was observed by SEM, and the microstructure of the composite after rapid thermal processing was also observed. The mechanical properties of SMPIC were characterized by Zwick tensile machine, among them, the samples were prepared according to ASTM-D3039 standard, and the tensile rate was 5 mm / min. The thermal-actuated shape memory testing was that, firstly, the SMPIC was put on the $T_g + 30$ ℃ thermal environment to bend to 180 °, then, the sample was cooled to the room temperature and obtained the temporary bending angle θ_1. After that, it was actuated in the $T_g + 30$ ℃ again to return to the original shape till the angle did not change and obtained the recovered bending angle θ_2. The equation of the shape fixation ratio (R_f) and shape recovery ratio (R_r) were as follows:

$$R_f = \frac{\theta_1}{180^\circ} \times 100\% \cdots\cdots \quad (2)$$

$$R_r = \frac{\theta_2}{\theta_1} \times 100\% \cdots\cdots \quad (3)$$

3. Results and discussion

3.1. Thermomechanical properties, thermal stability and mechanical properties of SMPIC

Fig. 2**a** and Fig. 2**b** were the storage modulus (E') curves and loss factor ($tan\ \delta$) curves of the SMPIC composites, respectively. The temperature at the highest point of the loss factor curve represented the glass transition temperature (T_g), which was also the shape memory transition temperature (T_{trans}). In the Fig. 2**a**, the room temperature E' of SMPIC-10, SMPIC-15, SMPIC-20, SMPIC-25, and SMPIC-30 were 4915 MPa, 6494 MPa, 4083 MPa, 3043 MPa, and 3780 MPa, successively, so, the E' showed a trend of first increasing and then decreasing. $Mg(OH)_2$ was rich in hydroxyl groups and had strong hydrogen bond interaction with the polyimide molecular chains, which increased the rigidity of the SMPIC, thus, the E' increased continuously. When the filler particles increased from 20 wt% to 25 wt%, it was easy to form particle aggregation and stress concentration points, and the interface bonding energy between the resin matrix and carbon fiber fabric was also reduced, so that the rigidity of the polymer chains and E' of the SMPIC were

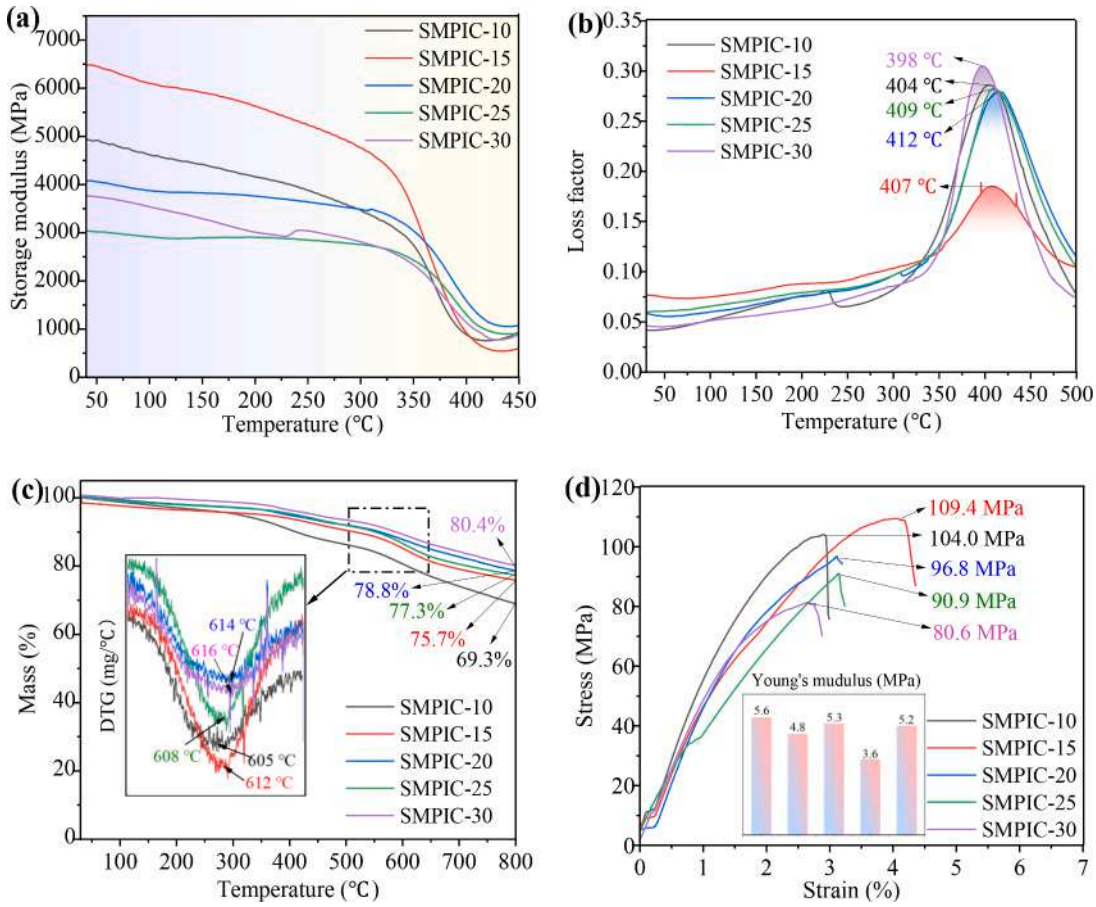

Fig. 2. (a) The storage modulus (E') curves of SMPIC, (b) the loss factor (tan δ) curves of SMPIC, (c) The TG curves of SMPIC, (d) the stress-strain curves, tensile strength and Young's modulus of SMPIC.

decreased. However, the *E'* of SMPIC-30 was higher than that of SMPIC-25, because $Mg(OH)_2$ belonged to inorganic rigid particles and had three functions: flame retardancy, smoke suppression, and filling. When it increased to 30 wt%, the particle amount was large, resulting in a higher storage modulus than that of SMPIC-25. In the Fig. 2**b**, the *tan δ* peaks were sharp between 375-425 ℃, and the highest peaks were at 398-412 ℃. The T_g of SMPIC-10, SMPIC-15, SMPIC-20, SMPIC-25, and SMPIC-30 were 404 ℃, 407 ℃, 412 ℃, 409 ℃, and 398 ℃, respectively, thus, the transition temperature increased first and then decreased. The reason was that with the amount of $Mg(OH)_2$ raising, the resistance to the molecular chains movement became stronger and stronger, and it required a higher temperature to move molecular chains, so, the T_g rose continuously. However, as the $Mg(OH)_2$ increasing to 25 wt%, it was easy to form particle aggregation, and the molecular chains rigidity was reduced. By contrary, the molecular chain segments flexibility was increased and could move at a lower temperature, macroscopically, the T_g was reduced.

Fig. 2**c** was the TG curves of the SMPIC, which showed that when the temperature was below 600 ℃, the TG curves dropped very slowly, indicating that the mass loss was very little. This was mainly caused by the decomposition of $Mg(OH)_2$, the evaporation of water vapor and the volatilization of small molecules. In the range of 600-800 ℃, SMPIC was decomposed rapidly, mainly due to the rapid decomposition of aromatic ring, aromatic heterocyclic ring and imide ring on the polyimide molecular main chains. When the temperature reached 800 ℃, the composite still had high residue ratio, specifically, the 800 ℃ residues of SMPIC-10, SMPIC-15, SMPIC-20, SMPIC-25, and SMPIC-30 were 69.3%, 75.7%, 77.3%, 78.8%, and 80.4%, respectively. The more the 800 ℃ residues was, the higher the thermal stability of the SMPIC had. Based on the previous research, the 800 ℃ residues of pure SMPI resin was 63.6% [31], so, the 800 ℃ residues of SMPIC was positively correlated with the filling amount of $Mg(OH)_2$. Because $Mg(OH)_2$ was decomposed into MgO and H_2O at high temperature, and H_2O was evaporated continuously. The boiling point of MgO was very high, up to 3600 ℃, which cannot be volatilized at 800 ℃ and remained in the composite, resulting in large residues.

The stress-strain curves in the Fig. 2**d** illustrated that the tensile strength of the SMPIC rose first and then decreased with the content of $Mg(OH)_2$ increasing. On one hand, SiO_2 and $Mg(OH)_2$ had strong hydrogen bonding interactions with the resin matrix and carbon fibers, on the other hand, the composite was designed to be a continuous "brick-and-mortar" structure, which could improve the mechanical properties. However, with $Mg(OH)_2$ particles amount increasing, the hydrogen bond association interactions were enhanced, further improving the cohesion between particles and forming stress concentration points, which made the mechanical strength decrease. Based on the previous research, the Young's modulus of SMPIC without $Mg(OH)_2$ (i.e. SMPI/CF) was 3.5 GPa [31]. Compared with the SMPI/CF composite, the Young's modulus of SMPIC in this paper was improved, which was related to the filled $Mg(OH)_2$ rigid particles.

3.2. *Microstructure of SMPIC*

The microstructure of the SMPIC composite was characterized by SEM. It can be seen from Fig. 3 that the SMPIC formed continuous "brick-and-mortar" layered structure similar to the nacre, in which carbon fiber fabric and SMPI matrix resin formed the continuous "hard brick" layer, and the $Mg(OH)_2$, SiO_2 particles and SMPI resin formed the "soft mortar" layer. Nacre was a kind of bioceramics, in which the "hard brick" in the "brick-and-mortar" structure was discontinuous, and it was

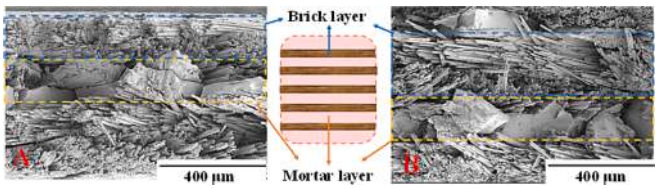

Fig. 3. SEM images of SMPIC, among them, A and B were SMPIC-10 and SMPIC-20, respectively.

easy to be cracked after rapid thermal processing. However, the continuous "hard brick" layer endowed SMPIC with high connectivity and mechanical properties, which made them less prone to fracture after rapid thermal processing. The reason is as follows: On one hand, the SMPI contains benzene rings, aromatic heterocycle and imide rings, which forms a large number of hydrogen bond interactions and π - π conjugate interactions with carbon fibers, improving the bonding ability between the resin and carbon fiber fabric. On the other hand, $Mg(OH)_2$ has a filling function and generates a large number of -OH groups, improving the compatibility with SMPI resin. In addition, multiple "hard brick" and "soft mortar" layers overlap with each other and form continuous "brick-and-mortar" multi-layer structures to enhance the connectivity.

3.3. Flame retardancy of SMPIC

The flame-retardant grade of SMPIC composite was determined by vertical combustion testing, and the results were shown in Table 1, which illustrated that the flame-retardant grade of all SMPIC composites reached V0. In the process of vertical combustion testing, the composite had no burning, no extending combustion, and just a little of fume. The more the $Mg(OH)_2$ amount was, the less smoke had, indicating that $Mg(OH)_2$ had flame retardancy effect. Additionally, SMPIC had self-extinguishing property without open flame combustion or droplet phenomenon, and cannot ignite the absorbent cotton, also, the surface of the material turned black and some areas turned white after burning. In order to quantitatively characterize the flame retardancy of SMPIC, we tested the LOI values, and as everyone known, the higher the LOI value was, the less flammable it was, and when the LOI was greater than 28%, the material was nonflammable. Fig. 4**a** showed that the LOI of SMPI/CF composite without $Mg(OH)_2$ was 48.9%, which was a refractory material, moreover, the LOI of SMPIC was all more than 50%, indicating that $Mg(OH)_2$ could improve the flame retardancy. Fig. 4**b** compared the LOI of polyimide composites in other literatures [32-39] in the past five years. It can be seen that the SMPIC composite had a tremendously high LOI and provided guarantee for applications in high temperature environment.

Fig. 4**c** shows the flame-retardant mechanism of SMPIC composite. First, $Mg(OH)_2$ can release bound water and absorb a large amount of latent heat energy during the thermal decomposition process to reduce the surface temperature of the composites. And it can inhibit the decomposition of polymer and cool the generated combustible gas. Second, MgO generated from $Mg(OH)_2$ is covered in the surface of SMPIC composite and together with SiO_2 to prevent the heat energy transferring to the interior materials. Third, the SMPIC has imitation nacre structures, of which the $Mg(OH)_2/SiO_2$/SMPI composite is equivalent to the "mortar" layer, and the carbon fiber/SMPI composite is equivalent to the "brick" layer, and multiple "brick-and-mortar" layers are stacked sequentially, which is to consume layer by layer. More importantly, the carbon fiber fabric is theoretically fire-resistant to 2600 ℃, which prevents the flame from spreading inwards. Fourth, the SMPI we synthesized contains a large amount of phenyl groups, which is easy to form a carbonized layer on the burned surface [40]. The carbonized layer is hard and dense, and effectively isolates the inner composite from high-temperature environment, thus slowing down the heat energy transfer and protecting the inner materials.

Table 1
Flame retardant grade of SMPIC composites.

Name	SMPIC-10	SMPIC-15	SMPIC-20	SMPIC-25	SMPIC-30
Flame retardant grade	V0	V0	V0	V0	V0

3.4. Ablation resistance of SMPIC

The ablation resistance of the SMPIC was tested using a cassette furnace ablation equipment (1350 ℃). Fig. 5**a** was the macro morphology of the SMPIC after ablation testing for 30 s, where A-E was SMPIC-10, SMPIC-15, SMPIC-20, SMPIC-25, and SMPIC-30, respectively. It showed that as the amount of $Mg(OH)_2$ increasing, the carbonization area (i.e. the white part) was gradually decreasing, and the ablation area was also reducing. Besides, SMPIC-20 was as an example to exhibit the ablation process for 30 s (Fig. 5**b**) and it had not been burned through, which indicated that the composite had great ablation resistance performance. This was mainly due to the continuous "brick-and-mortar" multi-layer structures, and the ablation mechanism was shown in Supporting Information, Section 1. In order to quantitatively characterize the ablation resistance of SMPIC composite, we tested the mass ablation rate, as shown in Fig. 5**c**. As the amount of the $Mg(OH)_2$ increasing, the mass ablation rate of SMPIC was declining continuously. Among them, the mass ablation rate of SMPIC-10 and SMPIC-20 were 0.01 g/s and 0.0053 g/s, respectively, of which the mass ablation rate decreased by 89%; the mass ablation ratio of SMPIC-30 was 0.0037 g/s, which was 170% lower than that of SMPIC-10.

FTIR was utilized to analyze the molecular structure change of the SMPIC composite after ablation testing, including center area, transition area and heat affect area, as shown in Fig. 5**d**. In the FTIR of the ablation transition area, the absorption peak of Mg-O bond is at 1365 cm^{-1}, the antisymmetric stretching vibration peak of Si-O-Si bond is at 1012 cm^{-1}, and the symmetric stretching vibration peak of Si-O bond is at 794 cm^{-1}. However, in the infrared spectrogram of the ablation center area, 1361 cm^{-1} is the characteristic absorption peak of Mg-O bond, while the absorption peak of Si-O bond disappears, because the SiO_2 is blown out under the high-speed heat flow scouring. Besides, the small absorption peaks at 1711 cm^{-1} and 1712 cm^{-1} are the vibration peaks of the -O-H bond in the absorbed water generated by the $Mg(OH)_2$. In the infrared spectrum of the heat affect area, the characteristic absorption peaks of polyimide are at 1774 cm^{-1}, 1706 cm^{-1}, 1351 cm^{-1} and 722 cm^{-1}. (The specific content was in the Supporting Information, Section 2.) The antisymmetric stretching vibration peak of Si-O-Si bond is at 1012 cm^{-1}, and the symmetric stretching vibration peak of Si-O bond is at 794 cm^{-1}. Therefore, it concludes that the resin matrix SMPI and SiO_2 in the heat affect area were intact; the SMPI matrix in the transition zone was carbonized, and SiO_2 still existed and the flame retardant $Mg(OH)_2$ was decomposed; by contrast, in the center area, the SMPI matrix was carbonized and $Mg(OH)_2$ generated MgO and H_2O, while SiO_2 was almost washed away by the high temperature heat flow, which was unable to be scanned by FTIR.

Fig. 5**e** showed 2D and 3D confocal microscope images of the ablation center area, transition area and heat affect area of SMPIC-20 after 30 s ablation testing. It can be seen that the spherical ablation products in the central ablation zone were the densest and the size was the smallest in the three areas. The number of spherical products in the transition zone was less than that in the central zone, but the size was larger than that in the central zone. However, the number of spherical products in the heat affect areas were the smallest and the size was the largest. This was because each area was affected differently by high-speed heat flow scouring, and the specific analysis was similar to the result of SEM-EDS.

In addition, SEM-EDS was used to characterize the microstructure of

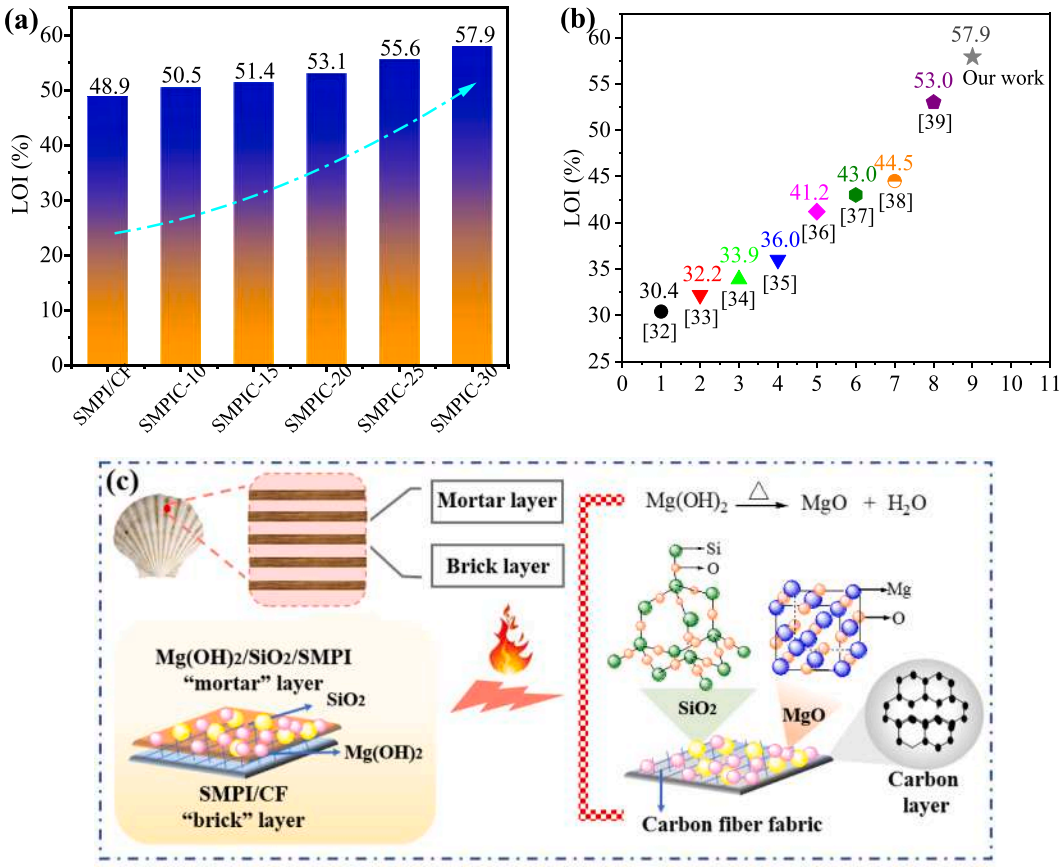

Fig. 4. (a) LOI statistical chart of SMPIC composites and SMPI/CF without flame retardant, (b) LOI comparison between SMPIC and other polyimide composites [32-39], (c) the flame-retardant mechanism of SMPIC.

the ablation center area, transition area and heat affect area of SMPIC-20 composite after ablation testing, as shown in Fig. 5**f**. The spherical ablation products in the central ablation zone were small and dense with a diameter of about 100 μm, and the surface was very smooth. The number of spherical ablation products in the transition zone was less than that in the central zone, and the diameter of the globules was about 200 μm, and some had smooth surfaces and some had rough surfaces. By contrast, the number of globules in the heat affect zone were the least with a diameter of about 300 μm, and the surface was very rough. Besides, according to the analysis of EDS and Mg, Si element distribution images, the level of Mg and Si elements increased continuously from the ablation center to the ablation edge. The reason was that the ablation center had the highest temperature and the surface resin changed into a molten state with good fluidity, while the sphere had the smallest surface Gibbs free energy, so tending to form spherical products. At the same time, $Mg(OH)_2$ was transformed into MgO and H_2O. After the rapid cooling process, the SMPIC entered the glass state from the molten state quickly, so that the water vapor cannot be discharged and the bubbles cannot break in time and remained in the spherical ablation products. In the ablation center area, the flame was perpendicular to the sample surface, with the highest flame temperature and the maximum high-speed scouring force caused by the gas flow, causing most of SiO_2 and part of MgO to be washed away. The transition region was scoured by vertical and parallel high temperature gas flow, although the temperature was lower than that of the central zone, $Mg(OH)_2$ was still transformed into MgO and H_2O. During the rapid cooling process, the ablation products changed from the molten state to the glassy state, and some water vapor cannot be discharged in time, producing larger bubbles. Also, the scouring force was lower than that in the central area, so the Mg and Si elements amounts were higher than that in the central area. As for the heat affect area, it was least affected by the heat flow, which had not enough energy to form a fully molten state and was more difficult to discharge water vapor, thus, the bubble diameter was the largest and the number was the least. In addition, as the flame moved from the transition zone to the edge zone, the temperature and the scouring force both decreased and the materials had the least damage, so the content of Mg and Si elements was the highest.

3.5. *Mechanical properties of SMPIC after rapid thermal processing*

Rapid thermal processing is a method of instantaneous uniform heating and cooling, which could characterize the mechanical properties of materials. The mechanical properties of the SMPIC composite after high temperature and rapid cooling process were shown in Fig. 6**a** and Fig. 6**b**. Compared with the original tensile strength, the tensile strength of the SMPIC composites decreased after rapid thermal processing at 600 ℃, but the degree of decline was not obvious; after rapid thermal processing at 800 ℃, the tensile strength decreased significantly. However, when the temperature difference was 1000 ℃, the tensile strength and the strength retention ratio increased except SMPIC-30. And the strength retention ratio of SMPIC-20 exceeded 100%, up to 103.3%, which was related to the continuous "brick-and-mortar" layered structure, flame retardant and SMPI carbonization. When the temperature difference reached 1350 ℃, the tensile strength decreased greatly, and the material was damaged seriously. In order to analyze the mechanical properties of SMPIC after rapid thermal processing, SEM was used to characterize the surface microstructures of SMPIC-20 and SMPIC-30.

Fig. 6**c** and Fig. 6**d** were the SEM images of the surface micromorphology of SMPIC-20 and SMPIC-30 after rapid thermal processing at different temperatures, respectively. For SMPIC-20 (Fig. 6**c**), when the temperature difference was 600 ℃, there were few pores on the surface,

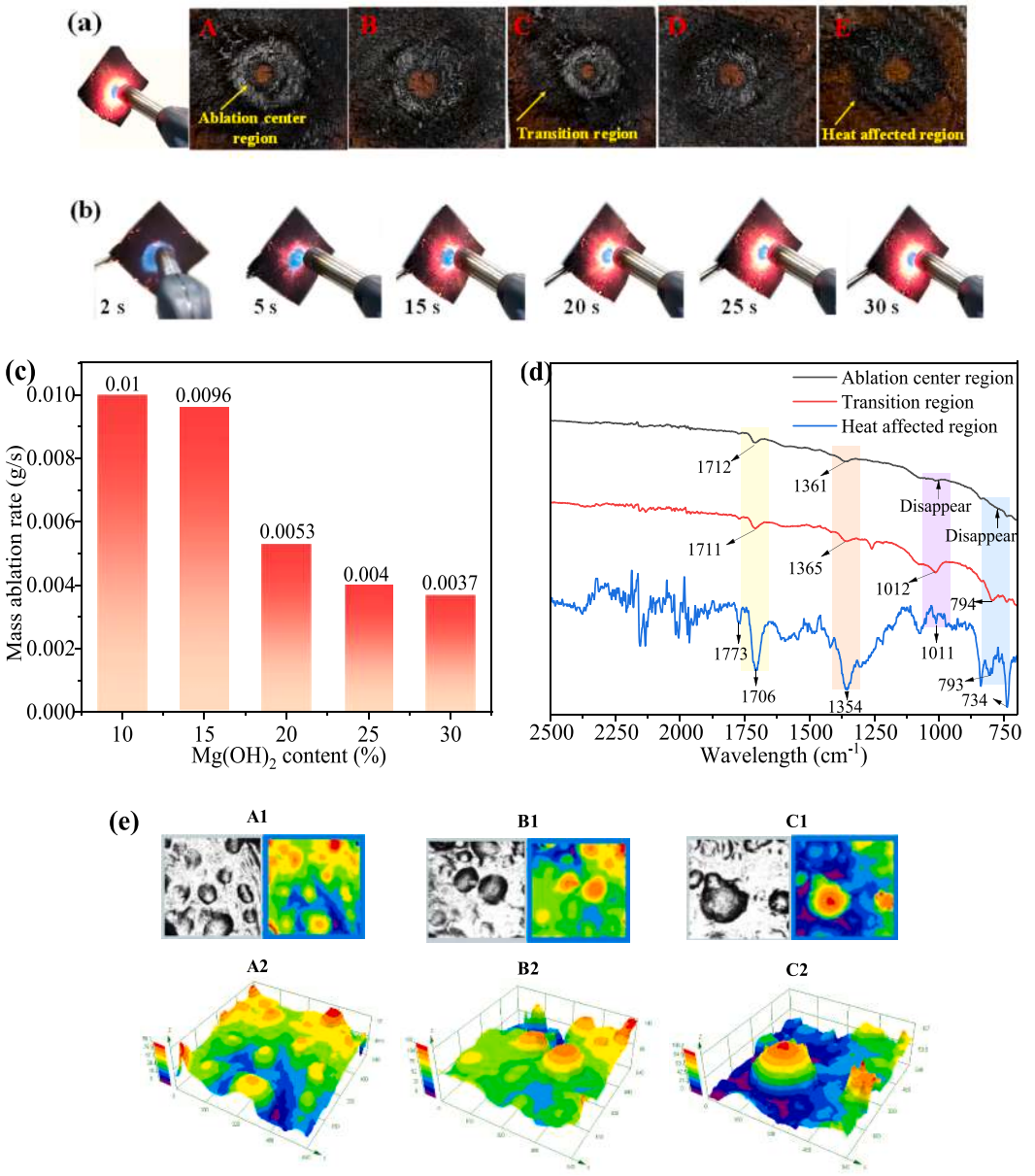

Fig. 5. (a) Photos of SMPIC composites after ablation for 30 s, (b) the ablation process of SMPIC-20, (c) the mass ablation rate of SMPIC, (d) FTIR spectrum of SMPIC-20 after ablation, (e) 2D (bright and colorful) and 3D confocal microscope images of SMPIC-20, where A1 and A2 were ablation center areas, B1 and B2 were transition areas and C1 and C2 were heat affect areas, (f) SEM-EDS images of SMPIC-20 after ablation, where A was the ablation central area, B was the transition area and C was the heat affect area.

and the resin and filler particles were combined closely. After 800 ℃ temperature difference treatment, the surface microstructure became loose, and the pores were small and dense, and some polyimides were carbonized and covered in the surface like floccule. Because the volatilization of H_2O molecule accelerated, which caused some volatilizing pore channels on the sample surface, and it cannot form an effectively protective layer. According to Griffith theory, these pores can produce microcracks under low external stress, causing catastrophic damage to the strength of the composites. With the temperature difference increasing to 1000 ℃, the material formed a dense surface micro morphology with almost no pore channels. This was mainly because SMPI contained a large amount of phenyl groups, which was easy to form a hard and dense carbonized layer and had good mechanical properties, also, the carbonized layer was wrapped with $5MgO \cdot 4CO_2 \cdot xH_2O$, MgO and SiO_2 particles, which together formed a dense and high temperature resistance surface microstructure, thus, the tensile strength and the strength retention ratio can be improved. When the temperature difference increased to 1350 ℃, $5MgO \cdot 4CO_2 \cdot xH_2O$ was converted into MgO crystals through high-temperature burning, and H_2O and CO_2 were volatilized completely. Besides, the molecular chains of SMPI resin matrix were broken to form benzene rings, imide, CO_2 and other small molecules, which were volatilized under high temperature environment, making the surface of SMPIC-20 extremely rough. There were a large number of pore channels with a diameter of about 3-5 μm on the surface, causing the mechanical tensile properties to decrease seriously.

For SMPIC-30 (Fig. 6**d**), when the temperature difference was 600 ℃, the sample had no pores, and the resin and filler particles were combined tightly. Because the sample contained a large amount of Mg $(OH)_2$, and it was almost intact. After rapid thermal processing at 800 ℃, the surface morphology was similar to that of SMPIC-20 at 600 ℃,

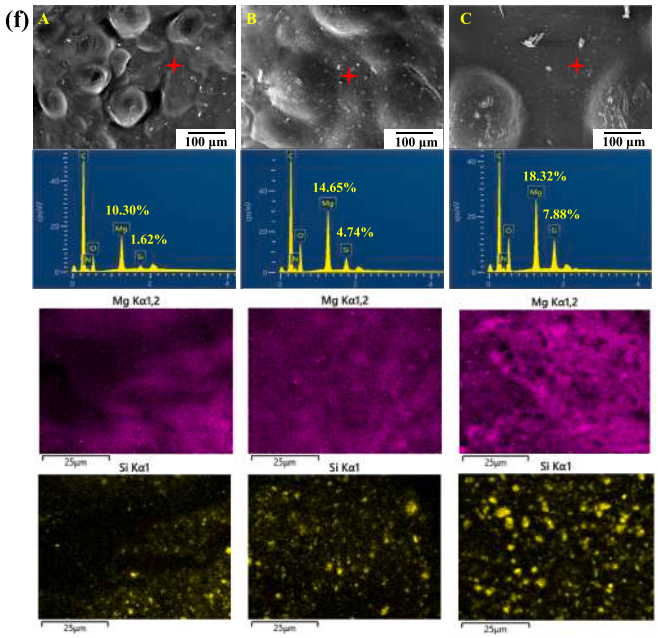

Fig. 5. (*continued*).

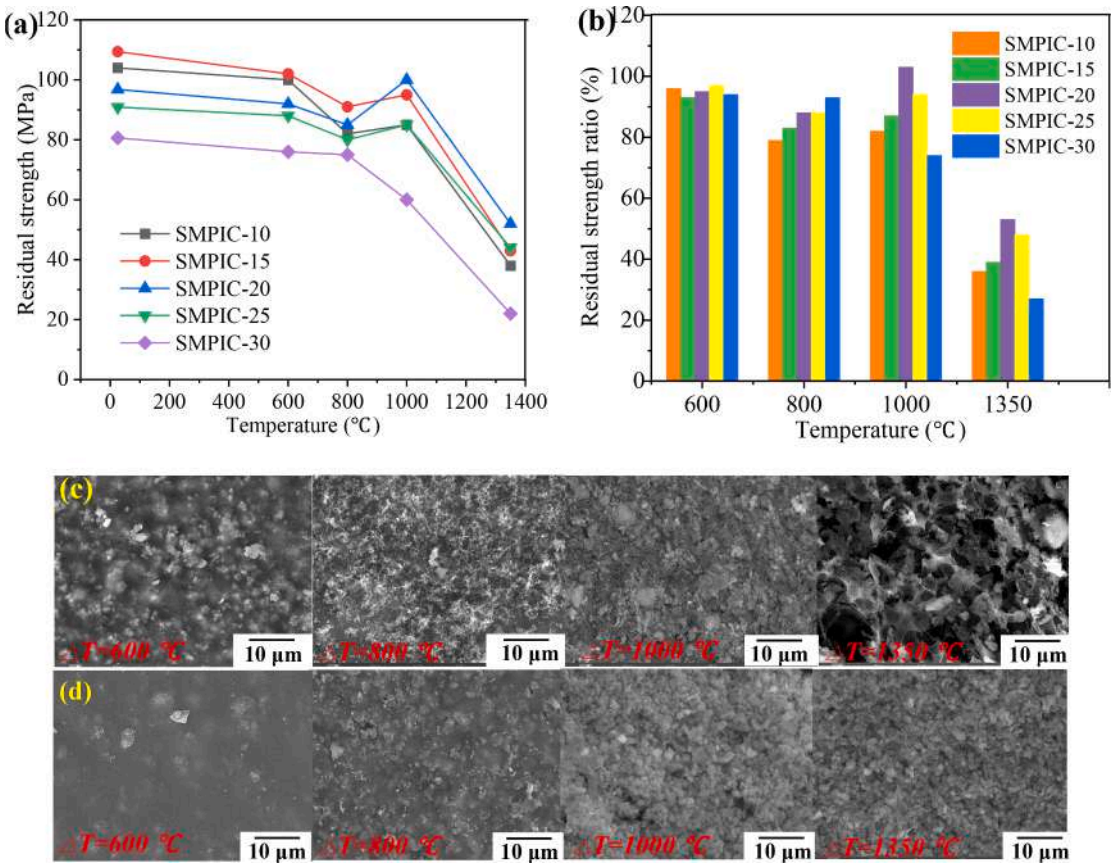

Fig. 6. (a) The residual tensile strength of SMPIC, (b) the retention ratio of residual strength of SMPIC, (c, d) SEM images of SMPIC-20 and SMPIC-30 after rapid thermal processing at different temperatures, respectively.

indicating that $Mg(OH)_2$ had excellent flame retardancy, which prevented some SMPI resins from burning. When the temperature difference was 1000 ℃, the sample surface was covered with dense particles, and some cavities and cracks appeared, which should be relevant to the increase of fillers and the decrease of the proportion of matrix resin. After rapid thermal treatment, the resin cannot form a continuous phase and the volatilization rate of H_2O and CO_2 was high, which resulted in many pore channels, also, the sample was shrunk sharply and generated a lot of cracks and stress concentration points, leading to the mechanical performance reduction. However, when the temperature difference

reached 1350 ℃, there were several small holes and dense filler particles on the surface. Because a large amount of $5MgO \cdot 4CO_2 \cdot xH_2O$ volatilized crystal water and carbon dioxide through high temperature environment, and transformed into MgO crystals and covered in the composite's surface together with SiO_2. According to Griffith theory, these small porosity defects can produce microcracks under low external stress, which caused catastrophic damage to the mechanical properties of SMPIC-30.

3.6. Shape memory properties of SMPIC

Through the testing and analysis of the above thermal mechanical properties, thermal stability, flame retardancy, ablation resistance, and the mechanical properties after rapid thermal treatment, it was shown that SMPIC-20 had excellent comprehensive properties, thus, taking SMPIC-20 as an example, shape memory process was shown in Fig. 7**a** and Fig. 7**b**. Under 442 ℃ thermal environment, SMPIC-20 can be shaped 90 ° and 180 ° under the external force. Then, the sample was put in the normal temperature, which could hold the temporary shape after removing the external force. Finally, when reheated to the 442 ℃ again, SMPIC-20 returned to the original shape. The 90 ° bending recovery time was 38 s and the 180 ° bending recovery time was 60 s, in contrast with SMPI/CF composite without flame retardant [31], the response time was reduced by 20 s. (The shape recovery process of SMPI/CF composite was shown in Supporting Information, Scheme 1.) And the shape fixation ratio and shape recovery ratio of the SMPIC sample were 93.5% and 92.6%, respectively. The flame retardant $Mg(OH)_2$ can be dehydrated at 300 ℃ to form MgO that was a metal oxide thermal conductive particle and had good thermal conduction ability, which was beneficial for the transfer of heat energy in the composite, thus, the response time of the SMPIC composite was decreased. Additionally, we made a simple actuator based on SMPIC-20, as shown in Fig. 7**c**. It took only 180 s to overturn an iron block that was 8 times more than its own weight. The process of the sample actuator overturned an iron block was shown in Supporting Information, video 1.

The shape memory mechanism of SMPIC composite was shown in Fig. 7**d**. The shape memory effect mainly came from the staged molecular chains structure changes of resin matrix and fibers along with the temperature changing, containing the transition of resin matrix between glass state and high elastic state, and the transition of fiber between leveling and buckling. Thermal-actuated shape memory process was divided into three stages: (I) Programming stage: when the temperature was higher than T_g of the SMPIC, the SMPI resin entered a high elastic state, meanwhile, the shear modulus was decreased and the bending resistance ability was poor. When the nominal bending strain of the SMPIC increased to the critical strain, the carbon fiber fabric could not be effectively fastened by matrix resin and was compelled to buckle in the compression zone, resulting in a large bending deformation for the SMPIC. (II) Fixation stage: while holding the external force and maintaining the bended status, cooling down the temperature to below T_g could restrain the molecular chains of the resin matrix. Meanwhile, the SMPI resin became hard, and the shear modulus rose, so that the matrix can effectively constrain the fiber without external force. (III) Recovery stage: when the temperature rose over the T_g of the SMPIC, the shear modulus of the SMPI resin decreased once more, so that the elastic potential energy locked in the constrained carbon fiber fabric was released. Also, the strain energy locked in the SMPI resin was released, macroscopically, the SMPIC returned to its original state. More importantly, MgO was an excellent thermal conductive material, which could decrease the surface thermal resistance and enhance the thermal conductivity of SMPIC and accelerate the heat transfer rate in the SMPI matrix, as a result, the reversible phase molecular chain segment motion

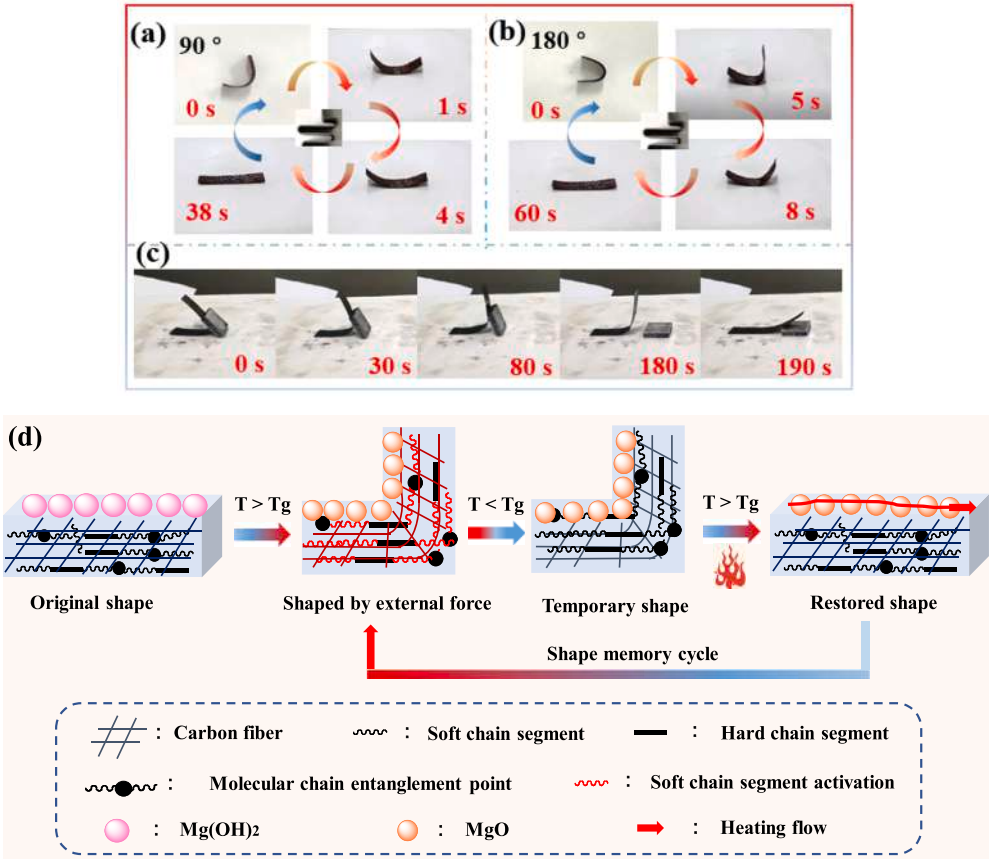

Fig. 7. (a) The shape recovery process of SMPIC-20 after bending 90°, (b) the shape recovery process of SMPIC-20 after bending 180°, (c) the sample actuator prepared by SMPIC-20 overturned an iron block, (d) the shape memory mechanism of SMPIC composite.

accelerated "thawing" and the shape response time was also decreased.

4. Conclusions

Based on the continuous "brick-and-mortar" layered structure inspired by nacre, we have successfully prepared a flame-retardant shape memory polyimide composite by hot pressing and secondary curing. When the content of flame retardant $Mg(OH)_2$ was 20%, the SMPIC had the best comprehensive properties, including the T_{trans} of 412 ℃, the tensile strength of 96.8 MPa, the flame-retardant grade of V0, and the LOI of 53.1%. Also, it had excellent high temperature airflow erosion resistance, when the temperature was 1350 ℃ for 30 s, the mass ablation ratio was 0.0053 g/s; after rapid thermal treatment at 1000 ℃, the tensile strength was 100 MPa, and the strength retention ratio was 103.3%. Besides, the shape fixation ratio and shape recovery ratio were 93.5% and 92.6%, respectively, and the simple actuator made by SMPIC-20 can overturn iron blocks that was more than 8 times of its own weight. Therefore, this work provided a reliable strategy for the construction of lightweight, high-performance and multi-functional smart composite, which can be applied to active deformation wings, active morphing re-entry parachute and other structures for high temperature environment.

CRediT authorship contribution statement

Xiaofei Wang: Data curation, Investigation, Methodology, Visualization, Writing – original draft, Writing – review & editing. **Yang He:** Investigation, Methodology, Project administration, Resources, Validation, Writing – review & editing. **Xinli Xiao:** Project administration, Resources, Validation, Writing – review & editing. **Yanju Liu:** Funding acquisition, Project administration, Supervision, Writing – review & editing. **Jinsong Leng:** Conceptualization, Funding acquisition, Project administration, Supervision, Writing – review & editing.

Declaration of competing interest

The authors declare that they have no known competing financial interests or personal relationships that could have appeared to influence the work reported in this paper.

Data availability

Data will be made available on request.

Acknowledgements

This research is supported by the National Key R&D Program of China (No. 2022YFB3805700), National Natural Science Foundation of China (No.92271206), and Science Foundation of National Key Laboratory of Science and Technology on Advanced Composites in Special Environments (No. 6142905222910).

Appendix A. Supplementary data

Supplementary data to this article can be found online at https://doi.org/10.1016/j.compositesa.2024.108151.

References

[1] Delaey J, Dubruel P, Van Vlierberghe S. Shape-memory polymers for biomedical applications. Adv Funct Mater 2020;30(44):1909047. https://doi.org/10.1002/adfm.201909047.
[2] Sun WJ, Liang HW, Zhang F, Li B. Theoretical study of the electroactive bistable actuator and regulation methods. Int J Smart Nano Mater 2022;14(1):36–56. https://doi.org/10.1080/19475411.2022.2152128.
[3] Hu JY, Jiang N, Du JK. Thermally controlled large deformation in temperature-sensitive hydrogels bilayers. Int J Smart Nano Mater 2021;12(4):450–71. https://doi.org/10.1080/19475411.2021.1958091.
[4] Tang ZZ, Gong JH, Cao PR, Tao LM, Pei XQ, Wang TM, et al. 3D printing of a versatile applicability shape memory polymer with high strength and high transition temperature. Chem Eng J 2022;431(2):134211. https://doi.org/10.1016/j.cej.2021.134211.
[5] Liu X, Ji H, Liu BY, Yang QS. All-solid-state carbon-nanotube-fiber-based finger-muscle and robotic gripper. Int J Smart Nano Mater 2022;13(1):64–78. https://doi.org/10.1080/19475411.2022.2028928.
[6] Miao WS, Zou WK, Jin BJ, Ni CJ, Zheng N, Xie T, et al. On demand shape memory polymer via light regulated topological defects in a dynamic covalent network. Nat Commun 2020;11(1):4257. https://doi.org/10.1038/s41467-020-18116-1.
[7] Ni CJ, Chen D, Yin Y, Wen X, Chen XL, Xie T, et al. Shape memory polymer with programmable recovery onset. Nature 2023;622:748–53. https://doi.org/10.1038/s41586-023-06520-8.
[8] Thomas TL, Bos J, Huaroto JJ, Venkiteswaran VK, Misra S. A magnetically actuated variable stiffness manipulator based on deployable shape memory polymer springs. Adv Intell Syst 2023:2200465. DOI: 10.1002/aisy.202200465.
[9] Xu LD, Zhao JT, Shi MF, Liu JB, Wang ZQ. Thermodynamic properties of TPI shape memory polymer composites reinforced by GO/SiO_2 modified carbon fiber. Compos Sci Technol 2022;226:109551. https://doi.org/10.1016/j.compscitech.2022.109551.
[10] Yang ZH, Zhang YM, Li S, Zhang XR, Wang TM, Wang QH. Fully closed-loop recyclable thermosetting shape memory polyimide. ACS Sustainable Chem Eng 2020;8(51):18869–78. https://doi.org/10.1021/acssuschemeng.0c05481.
[11] Wang XF, He Y, Liu YJ, Leng JS. Advances in shape memory polymers: remote-actuation, multi-stimuli-control, 4D printing and prospective applications. Mater Sci Eng R 2022;151:100702. https://doi.org/10.1016/j.mser.2022.100702.
[12] Kong DY, Li J, Guo AR, Xiao XL. High temperature electromagnetic shielding shape memory polymer composite. Chem Eng J 2021;408:127365. https://doi.org/10.1016/j.cej.2020.127365.
[13] Xie LL, Wang YX, Chen GC, Feng HJ, Zheng N, Xie T, et al. A thermadapt epoxy based on borate ester crosslinking and its carbon fiber composite as rapidly processable prepreg. Compos Commun 2021;28:100979. https://doi.org/10.1016/j.coco.2021.100979.
[14] Yao JN, Li TQ, Ma SQ, Qian GT, Song GL, Zhang JD, et al. Highly thermally stable and flexible conductive film electrodes based on photo-responsive shape memory polyimide. Smart Mater Struct 2020;29(11):115040. https://doi.org/10.1088/1361-665X/abb572.
[15] Huang ST, Sun LN, He MJ, Tang JL, Huang LQ. Preparation and properties of polyimide air-jet textured yarns and their woven fabrics. Text Res J 2019;90(13–14):1507–16. https://doi.org/10.1177/0040517519894391.
[16] Bai YJ, Yi XB, Li B, Chen SW, Fan ZJ. Constructing porous polyimide/carbon quantum dots aerogel with efficient photocatalytic property under visible light. Appl Surf Sci 2022;578:151993. https://doi.org/10.1016/j.apsusc.2021.151993.
[17] Stanford MG, Yang KC, Chyan Y, Kittrell C, Tour JM. Laser-induced graphene for flexible and embeddable gas sensors. ACS Nano 2019;13(3):3474–82. https://doi.org/10.1021/acsnano.8b09622.
[18] Xu LL, Xiao LH, Jia P, Goossens K, Liu P, Hui Li, et al. Lightweight and ultrastrong polymer foams with unusually superior flame retardancy. ACS Appl Mater Interfaces 2017;9(31):26392–9. https://doi.org/10.1021/acsami.7b06282.
[19] Madyaratri EW, Ridho MR, Aristri MA, Lubis MAR, Iswanto AH, Nawawi DS, et al. Recent advances in the development of fire-resistant biocomposites: a review. Polymers 2022;14(3):362. https://doi.org/10.3390/polym14030362.
[20] Cui XF, Zheng WJ, Zou W, Liu XY, Yang H, Yan J, et al. Water-retaining, tough and self-healing hydrogels and their uses as fire-resistant materials. Polym Chem 2019;10(37):5151–8. https://doi.org/10.1039/c9py01015g.
[21] Chen SM, Gao HL, Sun XH, Ma ZY, Ma T, Yu SH, et al. Superior biomimetic nacreous bulk nanocomposites by a multiscale soft-rigid dual-network interfacial design strategy. Matter 2020;1(2):412–27. https://doi.org/10.1016/j.matt.2019.03.012.
[22] Sun WB, Han ZM, Yue X, Zhang HY, Yang KP, Yu SH, et al. Nacre-inspired bacterial cellulose/mica nanopaper with excellent mechanical and electrical insulating properties by biosynthesis. Adv Mater 2023;35(24):2300241. https://doi.org/10.1002/adma.202300241.
[23] Zhang TF, Wang CF, Wang Y, Wang YL, Han ZD. Effects of modified layered double hydroxides on the thermal degradation and combustion behaviors of intumescent flame retardant polyethylene nanocomposites. Polymer 2022;14(8):1616. https://doi.org/10.3390/polym14081616.
[24] Wang X, Guo WW, Cai W, Wang JL, Song L, Hu Y. Recent advances in construction of hybrid nano-structures for flame retardant polymers application. Appl Mater Today 2020;20:100762. https://doi.org/10.1016/j.apmt.2020.100762.
[25] Mochane MJ, Mokhothu TH, Mokhena TC. Synthesis, mechanical, and flammability properties of metal hydroxide reinforced polymer composites: a review. Polym Eng Sci 2021;62(1):44–65. https://doi.org/10.1002/pen.25847.
[26] Wang CF, Liu JW, Wang YL, Han ZD. Enhanced flame retardance in polyethylene/magnesium hydroxide/polycarbosilane blends. Mater Chem Phys 2020;253:123373. https://doi.org/10.1016/j.matchemphys.2020.123373.
[27] Zhao PF, Zeng W, Yang ZW, Yang YX, Li J, Shi JP, et al. Preparation of a novel functionalized magnesium-based curing agent as an intrinsic flame retardant for epoxy resin. Chemosphere 2021;273:129658. https://doi.org/10.1016/j.chemosphere.2021.129658.
[28] Ni DW, Cheng Y, Zhang JP, Liu JX, Zou J, Chen BW, et al. Advances in ultra-high temperature ceramics, composites, and coatings. J Adv Ceram 2022;11(1):1–56. https://doi.org/10.1007/s40145-021-0550-6.
[29] Tang B, Wang Y, Hu L, Lin LB, Ma CX, Zhang CY, et al. Preparation and properties of lightweight carbon/carbon fiber composite thermal field insulation materials for

high-temperature furnace. J Eng Fiber Fabr 2019;14. https://doi.org/10.1177/1558925019884691. 1558925019884691.
[30] Chen SN, Li PK, Hsieh TH, Ho KS, Hong YM. Enhancements on flame resistance by inorganic silicate-based intumescent coating materials. Materials 2021;14(21):6628. https://doi.org/10.3390/ma14216628.
[31] Wang XF, He Y, Leng JS. Shape memory polyimides and composites with tunable chain stiffness and ultrahigh transition temperature range. Compos Part A: Appl S 2022;163:107237. https://doi.org/10.1016/j.compositesa.2022.107237.
[32] Wang L, Cui L, Fan J, Liu Y. Electrospun polyimide/organic montmorillonite composite nanofibrous membranes with enhanced mechanical properties and flame retardancy. J Ind Text 2020;49(7):875–88. https://doi.org/10.1177/1528083718801360.
[33] Xiong WW, Liu HT, Tian HF, Wu JL, Xiang AM, Wang CY, et al. Mechanical and flame-resistance properties of polyurethane-imide foams with different-sized expandable graphite. Polym Eng Sci 2020;60(9):2324–32. https://doi.org/10.1002/pen.25475.
[34] Tang W, Cao YF, Qian LJ, Chen YJ, Qiu Y, Xu B, et al. Synergistic charring fame-retardant behavior of polyimide and melamine polyphosphate in glass fiber-reinforced polyamide 66. Polymers 2019;11(11):1851. https://doi.org/10.3390/polym11111851.
[35] Qiao SY, Kang S, Zhu J, Wang Y, Yu JR, Hu ZM. A synergistic self-assembly strategy to fabricate thermally stable OPAN/PI composite aerogels for particulate matter removal. Mater Chem Front 2021;5(24):8308–18. https://doi.org/10.1039/d1qm00974e.
[36] Wu X, Wu L, Qi L, Yin LM, Yang Y, Jiang GL, et al. Preparation, characterization, and continuous manufacturing of nonflammable colorless and transparent semi-alicyclic polyimide film modified with phenoxy-phosphazene oligomer flame retardant. Express Polym Lett 2021;15(4):329–42. https://doi.org/10.3144/expresspolymlett.2021.29.
[37] Xue TT, Fan W, Zhang X, Zhao XY, Yang F, Liu TX. Layered double hydroxide/graphene oxide synergistically enhanced polyimide aerogels for thermal insulation and fire-retardancy. Compos Part B: Eng 2021;219:108963. https://doi.org/10.1016/j.compositesb.2021.108963.
[38] Liu HT, Tian HF, Yao YY, Xiang AM, Qi HS, Wang QX, et al. Polyimide foams with outstanding flame resistance and mechanical properties by the incorporation of noncovalent bond modified graphene oxide. New J Chem 2020;44(28):12068–78. https://doi.org/10.1039/d0nj01983f.
[39] Zhao YA, Chen JY, Lai XJ, Li HQ, Zeng XR, Jiang CC, et al. Efficient flame-retardant and multifunctional polyimide/MXene composite aerogel for intelligent fire protection. Compos Part A: Appl S 2022;163:107210. https://doi.org/10.1016/j.compositesa.2022.107210.
[40] Feng HS, Qian LJ, Lu L. Synergistic effect of polyimide charring agent and hexaphenoxycyclotriphosphazene on improving fire safety of polycarbonate: high graphitization to strengthen the char layer. Polym Advan Technol 2020;32(3):1135–49. https://doi.org/10.1002/pat.5161.